CI&CEQ
Chemical Industry & Chemical Engineering Quarterly

Available on line at
Association of the Chemical Engineers of Serbia *AChE*
www.ache.org.rs/CICEQ

Chem. Ind. Chem. Eng. Q. 23 (4) 483–493 (2017) CI&CEQ

ALI SAKIN[1]
IRFAN KARAGOZ[2]

[1]TOFAS-FIAT R&D Department, Istanbul Caddesi, Osmangazi, Bursa, Turkey
[2]Department of Mechanical Engineering, Uludag University, Nilufer, Bursa, Turkey

SCIENTIFIC PAPER

UDC 519.876.5:66:66.07

NUMERICAL PREDICTION OF SHORT-CUT FLOWS IN GAS-SOLID REVERSE FLOW CYCLONE SEPARATORS

Article Highlights

- Short-cut flows are mainly affected by vortex finder diameter and insertion length
- Insertion length has an optimum value for minimum short-cut flow
- Decrease in vortex finder diameter increases short-cut flow and pressure drop
- Short-cut flow increases with the cone tip diameter

Abstract

The effect of operational and geometrical parameters on the short-cut flow in cyclone separators has been investigated computationally using the Reynolds stress model (RSM). The motion of solid particles in the flow field was simulated using the Eulerian-Lagrangian approach with one way discrete phase method (DPM). Eleven cyclones with different cone tip diameters, vortex finder lengths and diameters were studied and the simulation results were analyzed in terms of velocity fields, pressure drops, cut-off diameters and short-cut flows. The numerical simulation was verified with the published experimental results. The results obtained demonstrate that all three parameters, particularly, vortex finder diameter, have significant effects on the cut-off diameter (collection efficiency), the short-cut flow and the pressure drop.

Keywords: CFD, cut-off diameter, pressure drop, separation efficiency, swirl flow.

A cyclone separator is a simple tool that leads the incoming solid-gas flow into a spiral motion and separates the solid particles from the main stream under the influence of centrifugal and gravity forces. Robust in structure, relatively inexpensive to construct and operate with little maintenance, cyclones are used for removal of harmful or nuisance air-borne particulates or liquid droplets. There are many versions of cyclone separators with various geometries and designs.

The major performance parameters of a cyclone separator are pressure drop and cut-off diameter values. Numerous theoretical and experimental studies carried out on this tough subject provide semi-empirical models varying from basic [1-4] to more comprehensive [5,6] for the prediction of a cyclone performance.

Several studies of small scale reverse flow cyclones have been undertaken by examining the effects of cyclone design and air flow rate on collection efficiency and pressure drop [7-10].

Optimization of cyclone performance by increasing cyclone separator collection efficiency and reducing the pressure drop was mainly derived from experiments rather than theoretical studies because the fluid motion in cyclones are complicated, including highly swirling turbulent characteristics and restrictions in the usage of empirical models [8,9,11-16].

Advances in computer capabilities, software and numerical methods provide more opportunities to computational calculation of cyclone separators [17-34].

Elsayed and Lacor performed numerical cyclone studies for the effect of cone tip diameter, dust bin geometry, vortex finder and inlet dimensions [28,31,35,36]. They reported that for the inlet dimensions effect of changing the inlet width on the cut-off diameter is more considerable than inlet height and optimum ratio

Correspondence: A. Sakin, TOFAS-FIAT R&D Department, Istanbul Caddesi, No:574 16369 Osmangazi, Bursa, Turkey.
E-mail: ali.sakin@tofas.com.tr
Paper received: 9 October, 2016
Paper revised: 4 January, 2017
Paper accepted: 13 January, 2017

https://doi.org/10.2298/CICEQ161009002S

of the inlet width to the inlet height is from 0.5 to 0.7 [36]. Regarding the cone tip diameter change, they reported that there is no significant effect on flow pattern and performance, and that decreasing the cone tip diameter increases the pressure drop [28]. Another study based on vortex finder dimensions, reported that reducing the vortex finder diameter by 40% leads to 175% increase in the dimensionless pressure drop (Euler number) and 50% reduction in the Stokes number [35]. In contrast with previous studies, they performed numerical cyclone analysis with Reynolds stress model (RSM) for investigation of dust outlet shape and reported that lack of dust outlet provides saving of large computational cost and it can affect the calculations in an error margin about 10% for the Euler number and 35% for the cut-off diameter [31].

Kaya and Karagoz [37] performed numerical studies to investigate performance characteristics of a cyclone prolonged with a dipleg and they reported that particle collection efficiency can be enhanced by applying a dipleg, which results in a variation in flow pattern for tangential inlet short cyclones. Increasing the dipleg length surface of the wall friction is increased which should lead to moderately lower tangential velocity.

Kaya *et al*. [38] investigated effects of surface roughness parameters on the performance of tangential inlet cyclones. Body diameter of 31 mm cyclone was utilized for numerical simulations by assigning different roughness values for inlet velocities 8 and 16 m/s, respectively. They concluded that the tangential velocity in the cyclone is decreased by increasing wall roughness, due to an increase in flow resistance and weakening of swirl so particle collection efficiency is deteriorated by greater surface roughness values. El-Batsh [39] performed CFD studies to improve performance of cyclone separator by appropriate selection of vortex finder dimensions. It was found that pressure drop is decreased with increasing vortex finder diameter and length of exit pipe is not a significant parameter on the cyclone performance.

Houben *et al*. [40] performed CFD simulations of cyclone separator with central vortex stabilization rod to suppress the vortex core precession and results were compared with the experimental data. They stated that the vortex is kept in position by using a stabilizer and maximum tangential velocity is found to be larger which has a positive effect on collection efficiency of small particles.

Haig *et al*. [41] performed CFD analysis on small scale cyclones with the body diameter of ranging from 29 to 52 mm and inlet flow rates ranging from 60 to 540 L/min. They stated that the capability of CFD accurately predicts performance indicators of pressure drop and collection efficiency.

Taking advantage of the increased availability of adjoint solvers in many commercial CFD codes, Elsayed [42] performed CFD analysis to find optimum shape of vortex finder. Resultant optimum vortex finder geometry provided reduction of 34% pressure drop and 83% cutoff diameter.

Song *et al*. [43] performed CFD analysis for D = = 290 mm and they investigated the influence of particle forces on separation efficiency. They analyzed effect of drag force, pressure gradient force, added mass force and Saffmann lift force. They stated that pressure gradient and added mass forces are at least 3 orders of magnitude smaller than the drag force and the Saffmann lift force is at least 15 orders of magnitude smaller. Therefore these forces can be neglected and the main driver of separation forces are drag and centrifugal forces.

The present study aims to investigate the effect of short-cut flow on the pressure drop and collection efficiency of reverse flow cyclone by changing cyclone tip diameter and vortex finder dimensions.

MATHEMATICAL MODEL AND NUMERICAL SIMULATION

Calculations were carried out on three cyclones with different cone tip diameters (fixed S and D_x values), four cyclones with different vortex finder lengths (fixed B_c and D_x values) and four cyclones with different vortex finder diameters (fixed S and B_c values). The dimensional layout and cyclone configurations are given in Figure 1 and Table 1.

Numerical method

The Eulerian-Lagrangian approach was used for numerical calculations of gas-solid flow in this study and flow is assumed as unsteady, incompressible and turbulent. Continuity and momentum equations are solved in order to obtain velocity field. The turbulent flow was represented by the Reynolds stress model (RSM) and particle trajectories and collection efficiencies were calculated by Lagrangian approach. Numerous particles that are injected from the inlet surface were followed through the flow field by solving the particle force balance equation of motion.

The flow field was defined as three-dimensional, the particle phase was assumed as dilute, and the particle loading level is low so interaction between the particles are insignificant and particles have no influence on the main stream flow. Therefore, the problem was assumed as one-way coupling [44]. By

this assumption, the source terms in Navier-Stokes equations due to two-way coupling strategy are not considered.

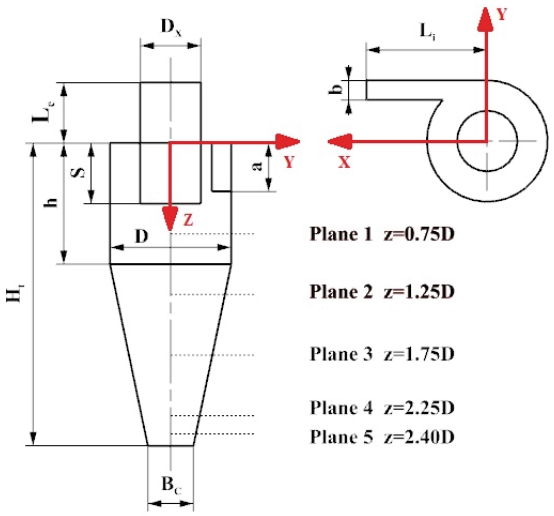

Figure 1. Schematic diagram of cyclone geometry and coordinate system definition.

Transport equations

The three-dimensional flow field in reverse flow cyclone was simulated using CFD. The conservation equations for mass and momentum in an incompressible Newtonian flow are as follows [45]:

$$\frac{\partial \rho}{\partial t} + \nabla(\rho \vec{v}) = S \tag{1}$$

$$\frac{\partial}{\partial t}(\rho \vec{v}) + \nabla(\rho \vec{v}\vec{v}) = -\nabla p + \nabla(\bar{\bar{\tau}}) + \rho \vec{g} + \vec{F} \tag{2}$$

where ρ is the fluid density, v is the fluid velocity, p is the static pressure, τ is the stress tensor ($= \mu[(\nabla \vec{v} + \nabla \vec{v}^T) - \frac{2}{3}\nabla \vec{v} I]$), μ is the molecular viscosity, I is the unit tensor, ρg is the gravitational body force, and F is the external body force.

The RSM was used to modify the viscous turbulent flow in reverse flow cyclone. The turbulent transport equation for RSM is [45]:

$$\frac{\partial}{\partial t}(\rho \overline{u_i' u_j'}) + \frac{\partial}{\partial x_k}(\rho u_k \overline{u_i' u_j'}) =$$
$$= -\frac{\partial}{\partial x_k}\left[\rho \overline{u_i' u_j' u_k'} + \overline{p(\delta_{kj} u_i' + \delta_{ik} u_j')}\right] +$$
$$+ \frac{\partial}{\partial x_k}\left[\mu \frac{\partial}{\partial x_k}(\overline{u_i' u_j'})\right] - \rho\left(\overline{u_i' u_j'}\frac{\partial u_j}{\partial x_k} + \overline{u_j' u_k'}\frac{\partial u_i}{\partial x_k}\right) - \tag{3}$$
$$-\rho\beta(g_i \overline{u_j'\theta} + g_j \overline{u_i'\theta}) + p\left(\frac{\partial u_i'}{\partial x_j} + \frac{\partial u_j'}{\partial x_i}\right)u_j' -$$
$$-2\mu \frac{\overline{\partial u_i' u_j'}}{\partial x_k \partial x_k} + S$$

where t is the time, u_i' is the fluctuating velocity to direction $i (= u_i - u_m)$, u_i is the velocity direction i, u_m is the mean velocity to direction i, $u_i' u_j'$ is the Reynolds stress tensor, β is the thermal expansion, p is the pressure, μ is the eddy viscosity, and S is the source term.

The two terms on the left-hand side of Eq. (3) indicate local time derivative and convection, res-

Table 1. Geometrical dimensions of cyclones; body diameter, D = 31 mm. Inlet length, L_i = 1.5D from the cyclone center, outlet length above cylindrical surface of cyclone is L_e = D

Dimension		Cyclone[a]	Dimension, D
Inlet height, *a*		-	0.4
Inlet width, *b*		-	0.16
Cylinder height, *h*		-	1.0
Total cyclone height, H_t		-	2.5
Cone tip diameter, B_c	$S = 0.5D$	CY1	0.625
	$D_x = 0.5D$	CY2	0.5
		CY3	0.375
Vortex finder length, *S*	$B_c = 0.375D$	CY4	0.4
	$D_x = 0.5D$	CY5	0.5
		CY6	0.875
		CY7	1.0
Vortex finder diameter, D_x	$B_c = 0.375D$	CY8	0.3
	$S = 0.5D$	CY9	0.4
		CY10	0.5
		CY11	0.645

[a]Cyclone CY3, CY5 and CY10 are identical

pectively from left to right. The terms on the right-hand side of Eq. (3) indicate turbulent diffusion, molecular diffusion, stress production, buoyancy production, pressure strain and dissipation respectively from left to right. The terms for turbulent diffusion, buoyancy production, pressure strain and dissipation are needed for modeling [46].

Discrete phase modeling

The motion of solid particles in a flow field was simulated using the Eulerian-Lagrangian approach with a discrete phase method (DPM). Gas phase was treated as continuum by Navier-Stokes equations and the solid phase is calculated. After flow field variables are obtained, particle tracking calculations are performed using Lagrangian approach. The volume fraction of the dispersed phase did not exceed 10%, so particle-particle interaction can be neglected and particle phase did not affect flow field (one-way coupling). A stochastic tracking method was used for modeling turbulent dispersion of particles. The trajectory of a particle can be calculated by integrating the force balance in a Lagrangian reference frame. This force balance equates the particle inertia with the forces acting on the particle, and can be written as [45]:

$$\frac{\mathrm{d}\vec{u}_p}{\mathrm{d}t} = F_D(\vec{u}-\vec{u}_p) + \frac{\vec{g}(\rho_p-\rho)}{\rho_p} + \vec{F} \tag{4}$$

where $\vec{F}$ is an additional acceleration (force/unit particle mass) term, $F_D(\vec{u}-\vec{u}_p)$ is the drag force per unit particle mass and:

$$F_D = \frac{18\mu C_D \mathrm{Re}_p}{24\rho_p d_p^2} \tag{5}$$

where u is the air velocity in a separator, u_p is the particle velocity, μ is the viscosity of air, ρ is the air density, ρ_p is the particle density, d_p is the particle diameter, Re is the relative Reynolds number, C_D is the drag coefficient and C_1 to C_3 are the constants that depends on the range of Re [47]:

$$C_D = C_1 + \frac{C_2}{\mathrm{Re}} + \frac{C_3}{\mathrm{Re}} \tag{6}$$

$$\mathrm{Re} = \frac{\rho d_p \left|u_p - u\right|}{\mu} \tag{7}$$

Numerical scheme

The selection of spatial and temporal discretization schemes has an important effect on the CFD results and fluent provides various solution strategies for pressure velocity coupling, pressure, momentum, kinetic energy, rate of kinetic energy dissipation discretization. Both Kaya and Karagoz [25] and Shukla *et al*. [30] analyzed various solution strategies in steady and unsteady simulations of cyclone separators. Based on the study of Kaya and Karagoz [25], governing equations of the three-dimensional, incompressible flow inside the cyclone, Eqs. (1) and (2), and the RSM turbulence equations were discretized over the computational cells and iteratively solved by using ANSYS Fluent commercial CFD software. SIMPLEC algorithm was used for pressure velocity coupling in this study and pressure staggering option (PRESTO) scheme was chosen for the pressure interpolation as it was shown to be well suited for steep pressure gradient involved in complex swirling flows. QUICK scheme was chosen for discretization of momentum, second order upwind scheme was chosen for turbulent kinetic energy and turbulent dissipation rate and first order upwind scheme was used for turbulence stresses.

Simulations started with steady solution, when convergence plot becomes nearly horizontal and there was no significant change, temporal discretization was switched to unsteady solution with the time step of 0.0001 s. Residence time values of cyclone configurations depending on inlet velocity are given in Table 2. Residence time exceeded for all simulations to prevent inconsistent results of flow field.

Boundary conditions and other settings

Velocity inlet boundary condition is employed at inlet, outflow at gas exit and wall (no-slip condition) at all other boundaries. Volumetric flow rate equals to 30 and 60 L/h, corresponding to air inlet velocity 8 and 16 m/s, respectively, dynamic viscosity of 2.11×10^{-5} Pa·s and air density 1.0 kg/m^3. The turbulence intensity and the hydraulic diameter were defined as 5% and 0.007 m, respectively. For the near wall treatment, scalable wall function was selected.

Table 2. Residence time and cell numbers

Parameter	CY1	CY2	CY3, CY4, CY5, CY6, CY7, CY10	CY8	CY9	CY11
Cyclone volume×10^3, m^3	0.0552	0.0521	0.0493	0.0456	0.0472	0.0532
t_{res} / s (U_{in} = 8 m/s)	0.1122	0.1059	0.1003	0.0927	0.0960	0.1082
t_{res} / s (U_{in} = 16 m/s)	0.0561	0.0529	0.0501	0.0463	0.0480	0.0541
Cell number	98582	95631	93756	92138	92556	96806

10^4 particles were released from the inlet surface with the air inlet velocity and a mass flow rate $\dot{m}_p$ of 0.001 kg/s and particle diameter varies from 0.5 to 10 μm. The density of released particles is 860 kg/m^3 and the maximum time steps number was 10^5 steps for each injection. The restitution coefficient was set as 0.8 for both normal and tangential direction. Trap DPM boundary condition was applied bottom surface of cyclone to calculate particle collection efficiency, escape was applied both inlet and outlet. The solution was assumed to be converged at each time step when preset scaled residuals reached 10^{-5} as convergence criteria for all variables. The calculations were carried out on an Intel® Core i7-2630QM 2.0 GHZ with 8 GB of RAM.

Solution of grid dependency

The flow volume was divided into a number of blocks by using Icem CFD 15.0 software to generate unstructured topology among the domain. However, fine mesh structure was used in the core region where strong gradients in the flow parameters were present. Grid independency was examined for CY3 cyclone. Three different grid domains containing 25.330, 93.756 and 349.222 cells were compared. The calculated grade efficiency curve with mesh design 349.222 cells is very close to mesh design with 93.756 cells and there is no appreciable difference in the prediction and mesh design with 93.756 cells is provided for computational solution. Grid independent cell numbers of other cyclone configurations were given in Table 2.

RESULTS

Model validation

Stairmand cyclones are widely used for industrial purposes so they became a significant research area from past to today. Hoekstra [48] studied barrel diameter of 290 mm and measured velocity profiles by LDA. This study is the newest one that can be taken as a reference for model validation. Xiang *et al.* [9] studied barrel diameter of 31 mm for various purposes and most of the studies, especially based on CFD, used this geometry due to small geometric domain and lower computational effort. It is also used for comprehensive optimization studies.

Calculated results were compared with the LDA velocity measurements of Hoekstra [48], measured by using laser Doppler anemometry (LDA) system. Figure 2 shows the comparison between RSM solution and the measured axial and tangential velocity profiles at axial station $z = 2.5D$ (Plane 3). As can be seen from Figure 2b, very good agreement was obtained for tangential velocity profiles at all planes. The axial velocity profiles do not agree well with the experimental values (Figure 2a). Considering complexity of the flow in cyclones, the agreement between the calculations and measurements is considered highly sufficient.

Calculation of short-cut flow rate

A small rate of mass flow directly moves toward the vortex finder by entering upward the vortex region. The short-cut flow rate strongly depends on cyclone separator parameters. To predict the short-

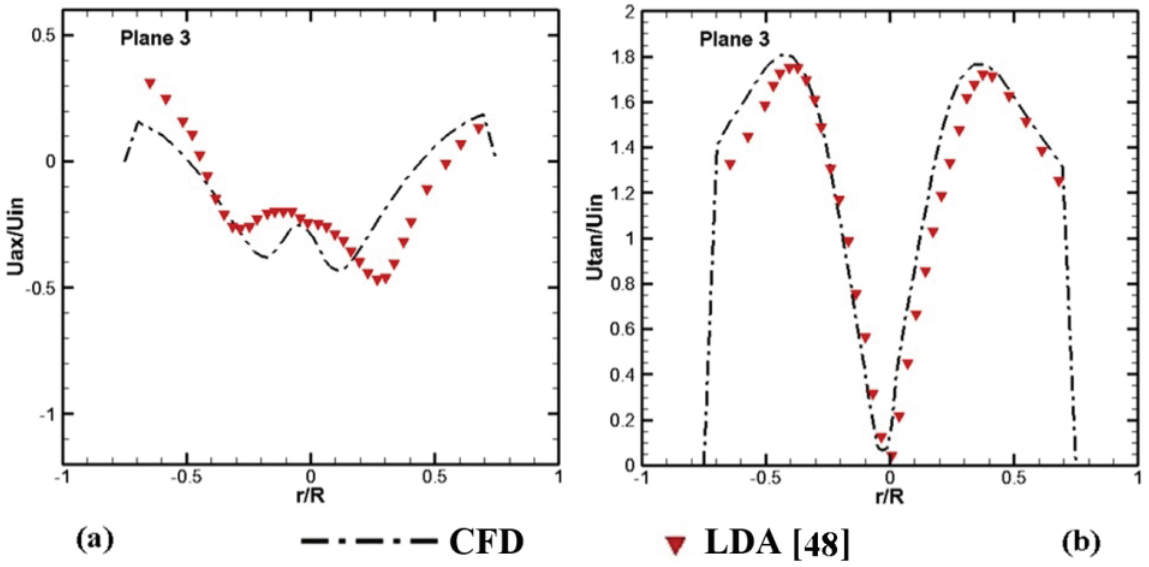

Figure 2. Comparison of axial (a) and tangential (b) velocity profiles between CFD results and LDA measurements (cyclone barrel diameter for validation study, D = 290 mm).

-cut flow rate, the downward flow rate at an axial station should be calculated instantly [49]. If the downward axial velocity is integrated between cyclone wall and the locus of zero at the axial station, the total downward flow rate is obtained. Since we create a new surface 1 mm below bottom of the vortex finder and clip axial velocity by locus of the zero and difference between downward and total flow rate in the cyclone will give the short-cut flow rate.

In this study, short-cut flow effect on cyclone performance is explained with tangential velocity profiles and short-cut flow rate. Tangential and axial velocity components have more significant effect on velocity field rather than radial velocity component. Tangential velocity component is more significant because it leads to centrifugal force for particle separation mechanism [49]. The axial flow has effect on downward and upward flows. To represent all velocity profiles for both inlet velocities and all five sections will create more pages so to prevent exceeding page number, velocity profiles at 1.75D section is presented for comparison of axial and tangential velocities for both inlet values.

Effect of cone tip diameter

Velocity profiles are given in Figure 3 represent the tangential and axial velocity distribution at z = 1.75D distance. The tangential velocity profiles show axis-symmetrical distribution for both inlet velocity values and inner region profiles are identical. The axial flows indicate existing of two flow streams: downward (positive axial velocity) and upward (negative axial velocity) directed to vortex finder exit.

Present CFD results of 8 m/s inlet velocity are in good agreement with LES [28] and for 16 m/s results are close to experimental data (Figure 4). Calculated cut off diameter differs from experimental data 41, 33 and 31% for CY1, CY2 and CY3, respectively. Elsayed and Lacor [31] observed that cyclone parameters are predicted without dust bin, an error margin around 10% in the calculations of Euler number and 35% in the calculation of cut-off diameter should be considered for CFD calculations.

Maximum collection efficiency is obtained for smaller cone tip diameter of 11.625 mm (CY3). Total friction surface area rates based on CY3 are 9.15% and 13.52% larger for CY2 and CY1 respectively, so maximum tangential velocity profiles of CY3 for both inlet velocities are higher than CY1 and CY2. This results stronger swirl intense and more centrifugal force for particle separation.

The short-cut flow increases with increasing cone tip diameter and this results in decreasing swirl intensity. While short-cut flow rate is increased, decreasing separation efficiency is expected but downward flow migration increases with increasing cone tip diameter so there is no significant change in the separation efficiency due to the change in cone tip diameter. In this case, maximum particle collection efficiency is obtained for maximum tangential velocity and minimum short-cut flow percentage.

The pressure drop values are in good agreement with experimental data and LES [28] calculations. Pressure drop increases with decreasing cone tip diameter as expected. Contrary to cut-off diameter,

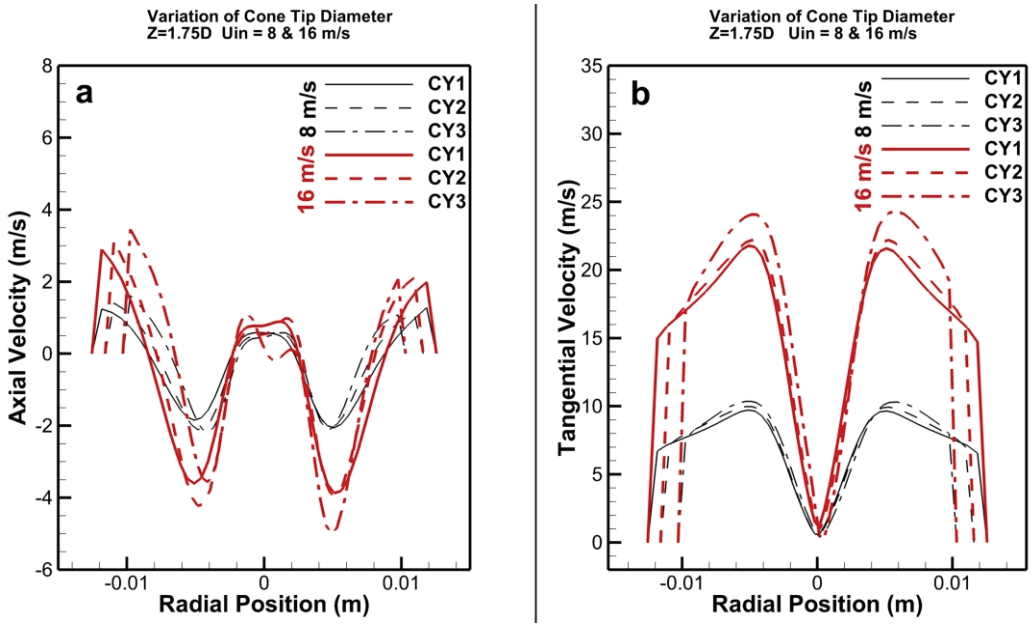

Figure 3. Comparison of axial (a) and tangential (b) velocity of CY1, CY2 and CY3 for Uin = 8 and 16 m/s at z = 1.75D section.

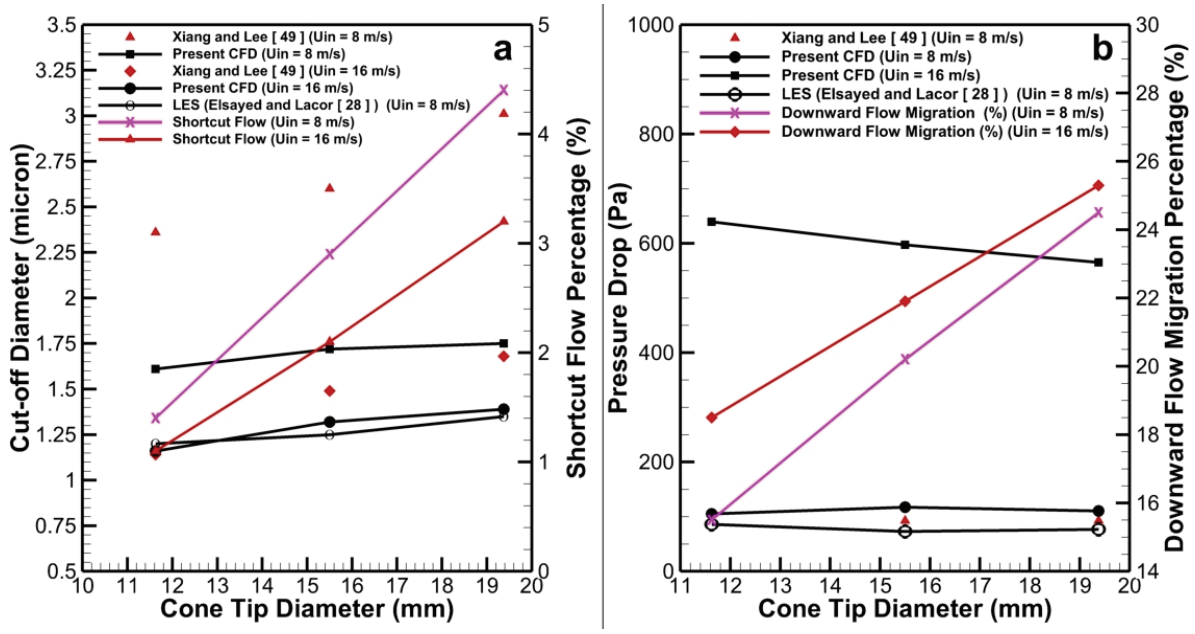

Figure 4. Cone tip diameter effects on cut off diameter, shortcut flow (a), pressure drop and downward flow (b). The results are compared to "Xiang and Lee [49]" literature [9].

pressure drop decreases with increasing short-cut flow due to weaker swirl in the flow field.

Effect of vortex finder length

In Figure 5, the tangential velocity profiles are quite similar. Maximum tangential velocity occurs at CY5 configuration ($s = 0.5D$) and maximum collection efficiency for both inlet velocities (Figure 6) is obtained for this configuration due to domination of tangential velocity on centrifugal force.

Shortest vortex finder (CY4, $s = 0.4D$) results increased short-cut flow so swirl intensity and pressure drop decrease concurrently. For this case, the inlet height (a) and vortex finder length (s) are equal and portion of inlet flow joins upward inner flow easily and short-cut flow rate is greater than CY5.

Only for small vortex finder length (CY4), axial velocity and downward flow through the cone is increased but at the same time separation efficiency is decreased due to increasing short-cut flow rate. CY5 has the optimum vortex finder length and results minimum short-cut flow and maximum efficiency.

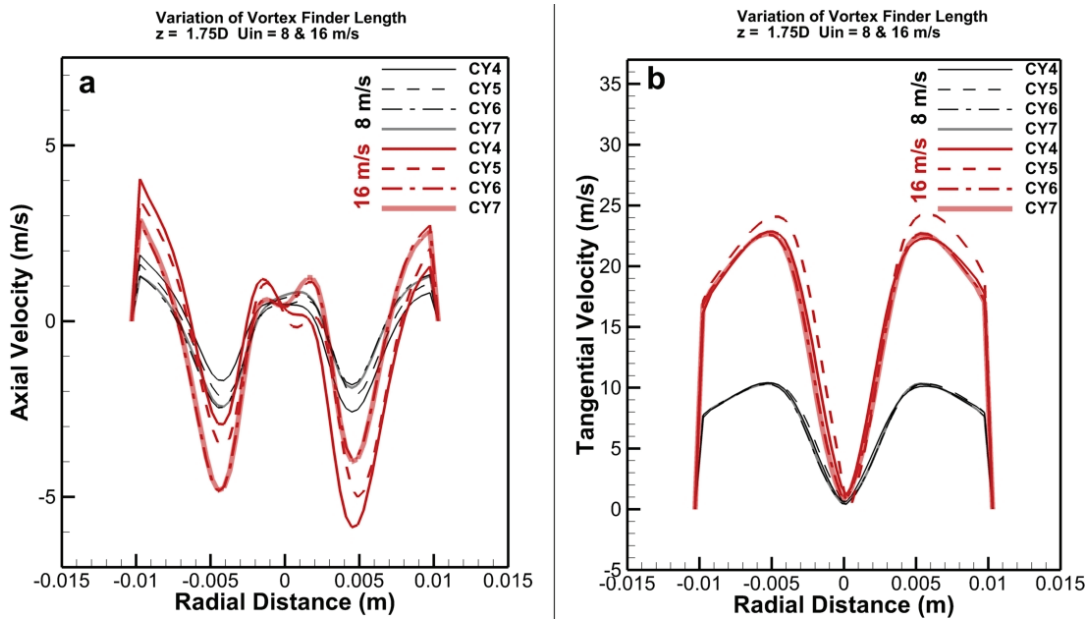

Figure 5. Comparison of axial (a) and tangential (b) velocity of CY4, CY5, CY6 and CY7 for Uin = 8 and 16 m/s at z = 1.75D section.

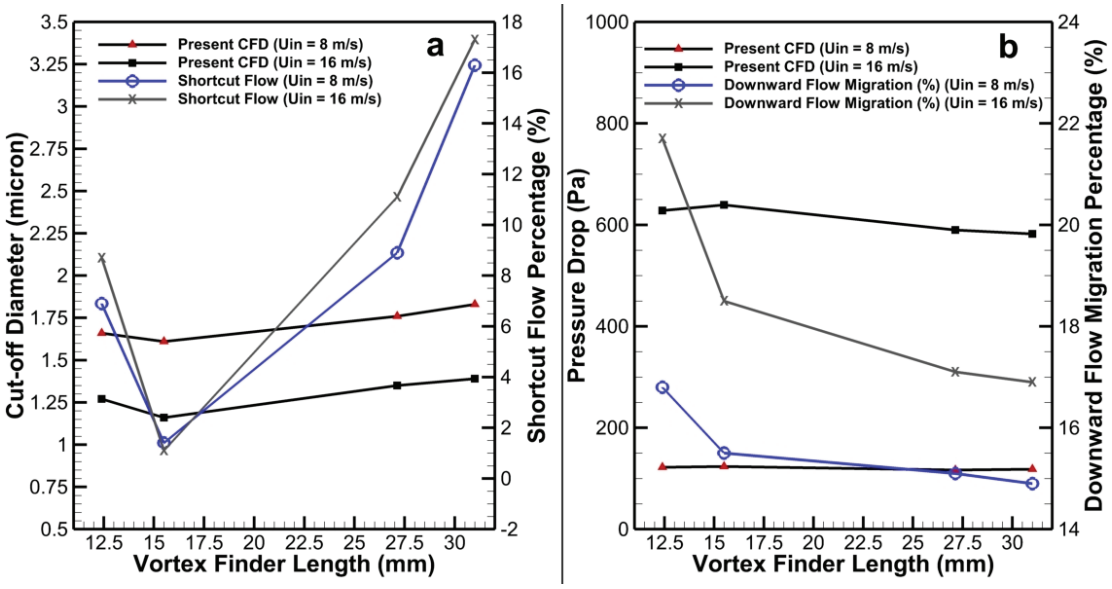

Figure 6. Vortex finder length effects on cut off diameter, shortcut flow (a), pressure drop and downward flow (b).

From the viewpoint of velocity profiles, CY5 has the maximum tangential velocity and pressure drop. Vortex finder of CY6 and CY7, extended into the cone section of cyclone, where the wall was contracting and flow coming from the cylindrical section, will be influenced by the contracting wall and easily join into the upward flow. The trend of short-cut flow rate is in good agreement with the explanation of Xiang and Lee [49]. The separation efficiency is decreased with decreasing tangential velocity and increasing short-cut flow rate for CY6 and CY7.

The pressure drop is increases with increasing tangential velocity and CY5 has the maximum pressure drop for both inlet values. Downward flow migration is decreased by increasing vortex finder length. Sharp decrease between CY4 and CY5 occurs and this can be explained by axial velocity profiles. For CY6 and CY7 both axial velocity profiles and downward flow rates are quite similar however swirl intensity is decreased with increasing friction surface.

Effect of vortex finder diameter

It can be clearly seen that maximum tangential velocity is decreased with increasing vortex finder diameter (Figure 7). From the viewpoint of tangential velocity profiles, cut off diameter is increased and pressure drop is decreased with increasing vortex finder diameter. Increased vortex finder diameter

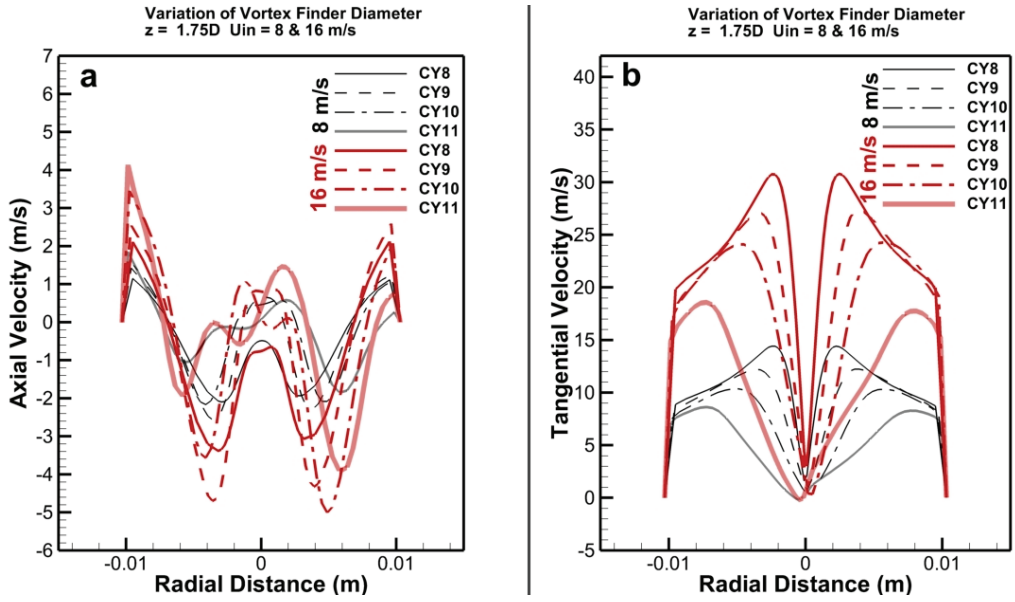

Figure 7. Comparison of axial (a) and tangential (b) velocity of CY8, CY9, CY10 and CY11 for Uin = 8 and 16 m/s at z = 1.75D section.

causes larger friction surface inside cyclone body so vortex strength (also tangential velocity which is the most dominant component for particle collection efficiency) is decreased.

Smaller vortex finder diameter (D_x) results the maximum separation efficiency although maximum short-cut flow rate occurs at the same time. The axial velocity profile demonstrates reversed W profile everywhere, but for small vortex finder diameter profile initially exhibits reversed V and becoming W at downward sections. Similar behavior was also reported by Elsayed and Lacor [35] and Hoekstra *et al.* [18]. Elsayed and Lacor [35] reported that this change results 73% increase in the maximum axial velocity. Hoekstra *et al*. [18] explained this situation; adverse pressure gradient leads to decay of swirl due to friction losses in the vortex finder. Swirl intensity increases for narrow vortex finder diameters, so that the adverse pressure gradient can be overcome.

Pressure drop is monotonically decreased for both inlet velocities as shown Figure 8. For smaller vortex finder diameters, pressure drop is increased due to increase in velocity and swirl intensity as explained previously and for larger vortex finder diameters pressure drop decreases with weaker swirl intensity. For CY8, downward flow rate is small in comparison with the others and this can be explained by the shape change of velocity profile. Downward flow rate is decreasing monotonically for CY9, CY10 and CY11 due to increased friction surface and weaker swirl intensity.

CONCLUSIONS

Cyclones of different cone tip diameters, vortex finder lengths and diameters were numerically analyzed using Reynold stress model (RSM). The following conclusions were obtained.

- Short-cut flow curve trend of cone tip diameter configurations at both inlet velocities are similar. Minimum short-cut flow rate is obtained for minimum cone tip diameter on contrary to maximum tangential velocity and pressure drop obtained with this cyclone configuration. Decreasing cone tip diameter increases separation efficiency, pressure drop, short-cut and downward flow concurrently.
- Vortex finder length has no significant effect on tangential velocity profile but shortest length causes increasing short-cut flow. $S = 0.5D$ is the optimum value for minimum short-cut flow and greater values result increasing short-cut flow due to contraction of conic cyclone walls. Downward flow migration is decreased with increasing vortex finder length due to increasing friction surface area.
- Vortex finder diameter has an important effect on cut-off diameter and tangential velocity. Increased vortex finder diameter results larger friction surface in cyclone body, weaker swirl intense and decreased pressure drop. $D_x = 0.3D$ is the smallest vortex diameter configuration and maximum short-cut flow and pressure drop is obtained due to velocity profile shape change from inverted “W” to inverted “V” shape.

From the viewpoint of short-cut flow rate, vortex finder dimensions (diameter and length) have more significant effect than cone tip diameter. Vortex finder

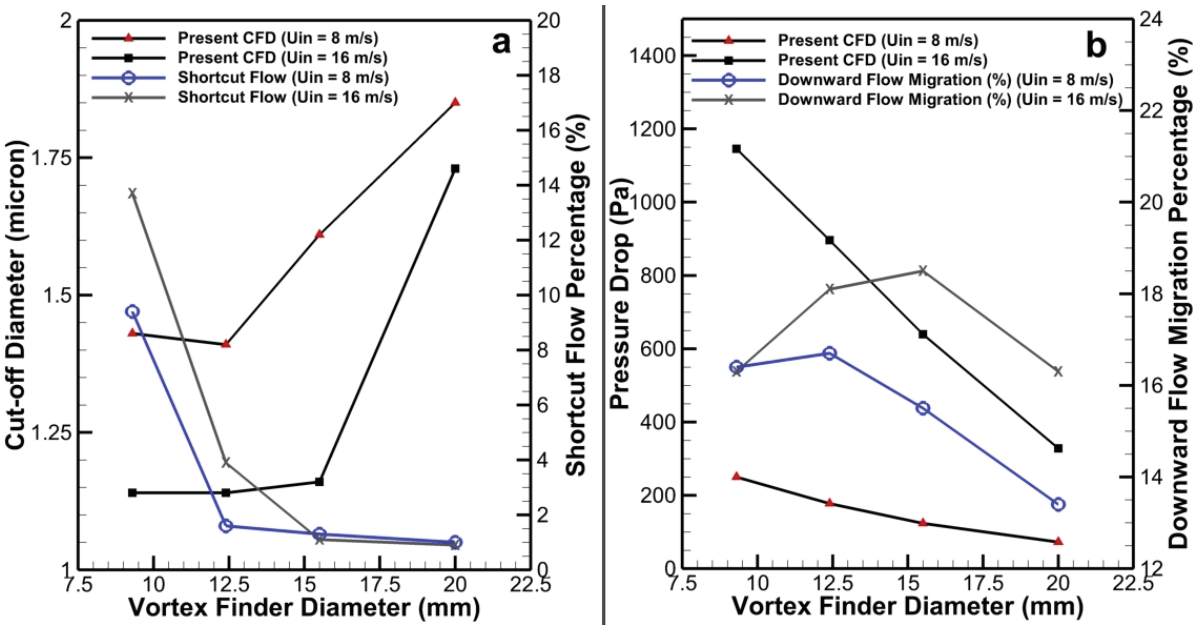

Figure 8. Vortex finder diameter effects on cut off diameter, shortcut flow (a), pressure drop and downward flow (b).

length of $0.5D$ is an optimum point for short-cut flow rate and for greater values of vortex finder length downward flow is joining upward flow due to contraction wall between cylindrical and conical section. Smaller vortex finder diameter causes change of velocity profile from "W" to "V" and short-cut flow percentage is increased.

As a recommendation of future work, numerical calculations can be carried out by modifying the cylinder and total height of the cyclone in order to investigate the effect of short-cut flow on pressure drop and particle collection efficiency.

Nomenclature

a	Inlet height of the cyclone
b	Inlet width of the cyclone
B_C	Cone tip diameter
C_1	Constant in Equation (6)
C_2	Constant in Equation (6)
C_3	Constant in Equation (6)
C_D	Particle drag coefficient
D	Cyclone body diameter
d_p	Particle diameter
D_X	Vortex finder diameter
F	External body force in Equation (2)
F	Additional acceleration term in Equation (4)
F_D	Drag force
g	Acceleration due to gravity
h	Cylinder height
H_t	Total cyclone height
I	Unit tensor
L_e	Outlet length above cylindrical surface of cyclone
L_i	Inlet length from the cyclone center
$\dot{m}_P$	Dust mass flow rate
p	Static pressure
$\mathrm{Re_p}$	Reynolds number based on the relative particle velocity
s	Vortex finder length
S	Source term in Equations (1) and (3)
t	Time
t_{res}	Residence time
u	Flow velocity component in i direction
u'	Fluctuating velocity component in i direction
u_p	Particle velocity
v	Fluid velocity
z	Section position in z direction

Greek

ρ	Fluid density
ρ_p	Particle density
μ	Molecular viscosity
τ	Stress tensor

Subscript

i	Cartesian coordinate
j	Cartesian coordinate
z	Cartesian coordinate
ax	Axial
in	Inlet
tan	Tangential

Abbreviations

CFD	Computational Fluid Dynamics
DPM	Discrete Phase Method
LDA	Laser Doppler Anemometry
LES	Large Eddy Simulation
PRESTO	Pressure Staggering Option
RSM	Reynolds Stress Model
SIMPLEC	Semi-Implicit Method for Pressure Linked Equations-Consistent
QUICK	Quadratic Upwind Interpolation

REFERENCES

[1] G.B. Shepherd, C.E. Lapple, J. Ind. Eng. Chem. **31** (1939) 972-984

[2] R.M. Alexander, Proc. - Australas. Inst. Min. Metall. **203** (1949) NS 152-153:203-228

[3] W. Barth, Brennst.-Waerme-Kraft **8** (1956) 1-9

[4] W. Barth, L. Leineweber, Staub - Reinhalt. Luft **24** (1964) 41-55

[5] A. Avci, I. Karagoz, J. Aerosol Sci. **34** (2003) 937-955

[6] I. Karagoz, A. Avci, Aerosol Sci. Technol. **39** (2005) 857-865

[7] J.C. Kim, K.W. Lee, Aerosol Sci. Technol. **12** (1990) 1003-1015

[8] M.E. Moore, A.F. McFarland, Environ. Sci. Technol. **27** (1993) 1842-1848

[9] R. Xiang, S.H. Park, K.W. Lee, J. Aerosol Sci. **32** (2001) 549-561

[10] Y. Zhu, K.W. Lee, J. Aerosol Sci. **30** (1999) 1303-1315

[11] L.C. Kenny, R.A. Gussman, J. Aerosol Sci. **28** (1997) 677-688

[12] C.J. Stairmand, Trans. Inst. Chem. Eng. **29** (1951) 356-383

[13] C.E. Lapple, Chem. Eng. **58** (1951) 144-151

[14] J. Dirgo, D. Leith, Aerosol Sci. Technol. **4** (1985) 401-415

[15] C. Köning, H. Büttner, F. Ebert, Part. Part. Syst. Charact. **8** (1991) 301-307

[16] S.L. Upton, D. Mark, W.D. Griffiths, J. Aerosol Sci. **25** (1994) 1493-1501

[17] J. Gimbun, T.G. Chuah, A. Fakhru'l-Razi, S.Y. Choong Thomas, Chem. Eng. Process. **44** (2005) 7-12

[18] A.J. Hoekstra, J.J. Derksen, H.E.A. Van Den Akker, Chem. Eng. Sci. **54** (1999) 2055-2065

[19] A.L. Gong, L.Z. Wang, Aerosol Sci. Technol. **38** (2004) 506-512

[20] T.G. Chuah, J. Gimbun, S.Y. Choong, Powder Technol. **162** (2006) 126-132

[21] L. Ma, D.B. Ingham, X. Wen, J. Aerosol Sci. **31** (2000) 1097-1119

[22] D.B. Ingham, L. Ma, Int. J. Energy Res. **26** (2002) 633--652

[23] I. Karagoz, F. Kaya, Int. Commun. Heat Mass Transfer **34** (2007) 1119-1126

[24] J.J. Derksen, H.E.A. Van den Akker, S. Sundaresan, AIChE J. **54** (2008) 872-885

[25] F. Kaya, I. Karagoz, Curr. Sci. **94** (2008) 1273-1278

[26] K. Elsayed, C. Lacor, Chem. Eng. Sci. **65** (2010) 6048--6058

[27] K. Elsayed, C. Lacor, Powder Technol. **212** (2011) 115--133

[28] K. Elsayed, C. Lacor, Comput. Fluids **51** (2011) 48-59

[29] J. You-hai, J. Guang-qin, C. Qing-yun, W. Jian-jun, Zhongguo Shiyou Daxue Xuebao, Ziran Kexueban **32** (2008) 109-112

[30] S.K. Shukla, P. Shukla, P. Ghosh, Adv. Powder Technol. **22** (2011) 209-219

[31] K. Elsayed, C. Lacor, Comput. Fluids **68** (2012) 134-147

[32] F. Qian, Z. Huang, G. Chen, M. Zhang, Comput. Chem. Eng. **31** (2007) 1111-1122

[33] H. Shalaby, K. Wozniak, G. Wozniak, Eng. Appl. Comput. Fluid Mech. **2** (2008) 382-392

[34] S.K. Shukla, P. Shukla, P. Ghosh, Eng. Appl. Comput. Fluid Mech. **5** (2011) 235-246

[35] K. Elsayed, C. Lacor, Comput. Fluids **71** (2013) 224-239

[36] K. Elsayed, C. Lacor, Appl. Math. Model. **35** (2011) 1952--1968

[37] F. Kaya, I. Karagoz, Chem. Eng. J. **151** (2009) 39-45

[38] F. Kaya, I. Karagoz, A. Avci, Aerosol Sci. Technol. **45** (2011) 988-995

[39] H.M. El-Batsh, Appl. Math. Model. **37** (2013) 5286-5303

[40] J.J.H. Houben, C. Weiss, E. Brunnmair, S. Pirker, J. Appl. Fluid Mech. **9** (2016) 487-499

[41] C.W. Haig, A. Hursthouse, D. Sykes, S. Mcilwain, Appl. Math. Model. **40** (2016) 6082-6104

[42] K. Elsayed, Sep. Purif. Technol. **142** (2015) 274-286

[43] C. Song, B. Pei, M. Jiang, B. Wang, D. Xu, Y. Chen, Powder Technol. **294** (2016) 437-448

[44] M. Sommerfeld, Theoretical and experimental modeling of particulate flow, Lecture Series 2000-6, von Karman Institute for Fluid Dynamics, 2000

[45] ANSYS Inc., ANSYS FLUENT 15.0 theory guide, Canonsburg, 2013

[46] S.K. Shukla, P. Shukla, P. Ghosh, Appl. Math. Model. **37** (2013) 5774-5789

[47] S.A. Morsi, A.J. Alexander, J. Fluid Mech. **55** (1972) 193--208

[48] A.J. Hoekstra, Gas flow field and collection efficiency of cyclone separators (Ph.D. thesis), Technical University Delft, 2000

[49] R.B. Xiang, K.W. Lee, Chem. Eng. Process. **44** (2005) 877-883.

ALI SAKIN[1]
IRFAN KARAGOZ[2]

NAUČNI RAD

NUMERIČKA PREDVIĐANJE STRUJNIH PREČICA U CIKLONSKIM SEPARATORIMA GASNO-ČVRSTO SA REVERSNIM TOKOM

Efekat operativnih i geometrijskih parametara na strujne prečice u ciklonskim separatorima istražen je pomoću modela Rejnoldsovih napona (RSM). Kretanje čvrstih čestica u strujnom polju simulirano je korišćenjem Ojler-Lagranžovog pristupa metodom diskretne faze u jednom smeru (DPM). Ispitivana su jedanaest ciklona sa različitim prečnicima konusa, dužinama i prečnicima vorteksa, a rezultati simulacije su analizirani u pogledu polja brzine, pada pritiska, kritičnog prečnika i strujnih prečica. Numerička simulacija je potvrđena već publikovanim eksperimentalnim rezultatima. Dobijeni rezultati pokazuju da sva tri parametra, a pre svega prečnik vorteksa, imaju značajne efekte na kritični prečnik (efikasnost sakupljanja), strujne prečice i pad pritiska.

Ključne reči: CFD, kritični prečnik, pad pritiska, efikasnost razdvajanja, kružni tok.